Theoretical study of stereodynamics for the $D' + DS(v = 0, j = 0) \rightarrow D'D + S$ abstraction reaction*

Guo Ya-Hui(郭雅慧)†, Zhang Feng-Yun(张凤昀), and Ma Hong-Zhang(马红章)

College of Science, China University of Petroleum, Qingdao 266555, *China*

(Received 17 October 2012; revised manuscript received 26 December 2012)

Quasiclassical trajectory (QCT) calculations have been performed for the abstraction reaction, $D' + DS(v = 0, j = 0) \rightarrow D'D + S$ on a new LZHH potential energy surface (PES) of the adiabatic $^3A''$ electronic state [Lü *et al.* 2012 *J. Chem. Phys.* **136** 094308]. The collision energy effect on the integral cross section and product polarization are studied over a wide collision energy range from 0.1 to 2.0 eV. The cross sections calculated by the QCT procedure are in good accordance with previous quantum wave packet results. The three angular distribution functions, $P(\theta_r)$, $P(\phi_r)$, and $P(\theta_r, \phi_r)$, together with the four commonly used polarization-dependent differential cross sections $((2\pi/\sigma)(d\sigma_{00}/d\omega_t)$, $(2\pi/\sigma)(d\sigma_{20}/d\omega_t)$, $(2\pi/\sigma)(d\sigma_{22+}/d\omega_t)$, $(2\pi/\sigma)(d\sigma_{21-}/d\omega_t))$ are obtained to gain insight into the chemical stereodynamics of the title reaction. Influences of the collision energy on the product polarization are exhibited and discussed.

Keywords: quasi-classical trajectory, integral cross section, stereodynamics, product polarization

PACS: 34.50.Lf, 82.20.–w, 82.20.Pm **DOI:** 10.1088/1674-1056/22/5/053402

1. Introduction

Recently, the reactions involving sulfur atoms and sulfur-containing species have attracted great attention for their important role in combustion and atmospheric chemistry. The dynamics of both $S(^3P)$ and $S(^1D)$ reaction with hydrogen molecules and its isotope variants have been investigated, and the electronic excitation effect on the reaction dynamics of atomic sulfur and the possible role of intersystem crossing between triplet and singlet potential energy surfaces have also been explored directly.[1–8] For instance, Shiina *et al.*[9] and Tsuchiya *et al.*[10] successively measured the thermal rate constant of the $S(^3P) + H_2$ and $S(^3P) + D_2$ reaction using a laser photolysis-shock tube-atomic resonance absorption spectrometry method and found a notable Arrhenius temperature dependence of the two reaction rate constants.

From the theoretical point of view, a sufficiently accurate potential energy surface is critical for elaborate dynamical calculations. The first global $H_2S(^3A'')$ PES was presented by Martin with the collinear transition state located at $R_{HH} = 2.6a_0$ and $R_{HS} = 2.6a_0$.[11] Then, many efforts have been made on the PES construction of the H_2S system since the first *ab initio* investigation. Maiti *et al.*[4] produced the PES for the H_2S ($^3A''$) state while evaluating the importance of intersystem crossing in the $S(^3P,^1D) + H_2$ reaction. Based on their own PES for the two lowest triplet states and the PES for the lowest singlet state developed by Ho *et al.*,[12] they have found that the location of the singlet/triplet crossing occurring on the reagent side of the triplet barrier dominates the thermal rate constant behavior at low temperatures. They also revealed that trajectories which undergo a triplet-to-singlet transition have higher product rotational excitation than those that remain on the triplet surfaces. In a following work, Klos *et al.*[3] fitted the analytical PES for $H_2S(^3A'')$. The statistical model of atom–diatom insertion reactions in combination with coupled-states capture theory was adopted to calculate integral cross sections for formation for specific rotational/fine-structure states of the product.

Compared with $S(^3P,^1D) + H_2$ reaction, the reverse abstraction reaction $H' + SH \rightarrow H'H + S$ and its isotope variants have been less extensively investigated. Until recently, Lü *et al.* have constructed a new *ab initio* LZHH PES for the lowest triplet state of $H_2S(^3A'')$ using the high-level multi-reference (MRCI+Q) method with a basis set of aug-cc-pV5Z.[13] The influences of collision energy and reagent vibrational excitation on the reactivity for $H' + SH$ and its isotope variant $D' + SD$ have also been carried out using an exact quantum dynamical study and quasi-classical trajectory calculations based on their own PES.[13,14] A good agreement between center-of-mass (CM) and quasiclassical trajectory (QCT) was found.

The previous work reported by Lü *et al.* mainly focused on scalar properties, e.g., integral cross section, reaction probability, and so on. As we know, the vector properties, such as velocity and angular momentum, possess not only magnitude that can be directly related to translational and rotational energies, but also well-defined directions.[15–21] Benefitting from the development of polarized laser techniques, information about the reagent/product alignment and orientation could be obtained.[22–24] However, there have been no studies

*Project supported by the National Natural Science Foundation of China (Grant Nos. 41201336 and 41001250) and the Fundamental Research Funds for the Central Universities of China (Grant No. 13CX02018A).

†Corresponding author. E-mail: yhguo@upc.edu.cn

© 2013 Chinese Physical Society and IOP Publishing Ltd

of the vector correlations (so-called stereodynamics) for the $D' + DS \rightarrow D'D + S$ abstraction reaction.

In this paper, we performed the QCT calculations on the $D' + DS \rightarrow D'D + S$ abstraction reaction using the recently developed $^3A''$ PES so as to study the effect of collision energy on the integral cross sections as well as stereodynamics characteristics. The calculated results have been compared with the available quantum mechanical (QM) results.

2. Computational details

The QCT methodology employed here is similar to that described in Refs. [25]–[27], and the method has been successfully adopted to explore a great deal of collision reactions.[28–40] The CM frame chosen in the calculations is plotted in Fig. 1. The reagent relative velocity vector $\boldsymbol{k}$ is parallel to the z axis, whereas the y axis is perpendicular to the x–z scattering plane (which contains the initial and final relative velocity vectors, $\boldsymbol{k}$ and $\boldsymbol{k}'$). The θ_t and θ_r refer to the scattering angle between the vector $\boldsymbol{k}$ and $\boldsymbol{k}'$, the polar angle between the vector $\boldsymbol{k}$ and $\boldsymbol{j}'$ (the product rotational angular momentum vector), respectively. The azimuthal angle between $\boldsymbol{j}'$ and $\boldsymbol{k}$–$\boldsymbol{k}'$ scattering plane is defined as ϕ_r. $\omega_t = \theta_t$, ϕ_t refers to the coordinates of the unit vector $\boldsymbol{k}'$ along the direction of $\boldsymbol{k}'$ in the CM frame. The full three-dimensional angular distribution associated with $\boldsymbol{k}$, $\boldsymbol{k}'$, and $\boldsymbol{j}'$ is represented with a set of generalized polarization-dependent differential cross sections (PDDCS) in the CM frame. The fully correlated CM angular distribution is written as[31]

$$P(\omega_t, \omega_r) = \sum_{kq} \frac{[k]}{4\pi} \frac{1}{\sigma} \frac{d\sigma_{kq}}{d\omega_t} C_{kq}(\theta_r, \phi_r)^*, \quad (1)$$

where $[k] = 2k + 1$, and $(1/\sigma)(d\sigma_{kq}/d\omega_t)$ is a generalized PDDCS. Four PDDCSs are taken into account, including $kq =$ (00), (20), (22+), and (21−). The four PDDCSs are denoted as $PDDCS_{00}$, $PDDCS_{20}$, $PDDCS_{22+}$, and $PDDCS_{21-}$ for convenience. The $C_{kq}(\theta_r, \phi_r)$ are modified spherical harmonics.

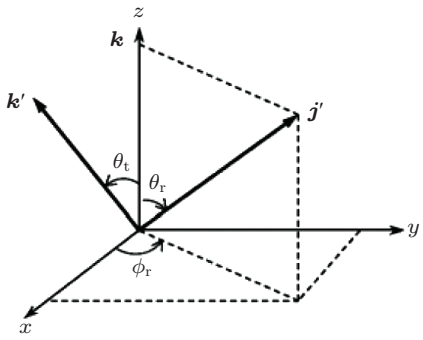


Fig. 1. Center-of-mass coordinate system describing the $\boldsymbol{k}$, $\boldsymbol{k}'$, and $\boldsymbol{j}'$ correlation.

The $\boldsymbol{k}$–$\boldsymbol{j}'$ angular distribution $P(\theta_r)$ is expressed by a series of Legendre polynomials as[41]

$$P(\theta_r) = \frac{1}{2} \sum_k (2k+1) a_0^{(k)} P_k(\cos\theta_r), \quad (2)$$

where

$$a_0^{(k)} = \int_0^{\pi} P(\theta_r) P_k(\cos\theta_r) \sin\theta_r \, d\theta_r = \langle P_k(\cos\theta_r) \rangle . \quad (3)$$

The coefficients $a_0^{(k)}$ are called orientation (k is odd) or alignment (k is even) parameters. The $k = 2$ indicates the product rotational alignment

$$a_0^2 = \langle P_2(\cos\theta_r) \rangle = \langle P_2(\boldsymbol{j}' \cdot \boldsymbol{k}) \rangle = \frac{1}{2} \langle 3\cos^2\theta_r - 1 \rangle . \quad (4)$$

The dihedral angle distribution function $P(\phi_r)$ describing $\boldsymbol{k}$–$\boldsymbol{k}'$–$\boldsymbol{j}'$ correlation can be expanded in Fourier series as[41]

$$P(\phi_r) = \frac{1}{2\pi} (1 + \sum_{\text{even},n\geq 2} a_n \cos n\phi_r + \sum_{\text{odd},n\geq 1} b_n \sin n\phi_r), \quad (5)$$

where

$$a_n = 2\langle \cos n\phi_r \rangle , \quad b_n = 2\langle \sin n\phi_r \rangle . \quad (6)$$

In this calculation, $P(\phi_r)$ is expanded to $n = 24$ for the convergence.

The joint probability density function of angles θ_r and ϕ_r, which determine the direction of $\boldsymbol{j}'$, can be written as

$$\begin{aligned} P(\theta_r, \phi_r) &= \frac{1}{4\pi} \sum_{kq} (2k+1) a_q^k C_{kq}(\theta_r, \phi_r)^* \\ &= \frac{1}{4\pi} \sum_k \sum_{q\geq 0} \left[a_{q+}^k \cos q\phi_r - a_{q-}^k \mathrm{i} \sin q\phi_r \right] C_{kq}(\theta_r, 0), \end{aligned} \quad (7)$$

where

$$a_{q+}^k = 2\langle C_{k|q|}(\theta_r, 0) \cos q\phi_r \rangle , \quad (k \text{ is even}), \quad (8)$$

$$a_{q-}^k = 2\mathrm{i}\langle C_{k|q|}(\theta_r, 0) \sin q\phi_r \rangle , \quad (k \text{ is odd}), \quad (9)$$

and $C_{kq}(\theta_r, \phi_r)$ are modified spherical harmonics. In our computation, $P(\theta_r, \phi_r)$ is expanded to $k = 7$ to guarantee the convergent results.

The QCT calculations have been carried out on the $^3A''$ PES.[13] The transition state for the title reaction is collinear and the reaction on $^3A''$ state proceeds without a well. As obtained from analytical PES, the transition state located at $R_{HH} = 2.54a_0$ and $R_{HS} = 2.62a_0$ with a higher barrier of 0.09 eV (the zero-point energy difference is not considered) compared with the pre-determined value of 0.078 eV fitted by Maiti *et al.* Meanwhile, Maiti *et al.* utilized the 3D-spline interpolation method to construct the PES of the interaction areas based on the quadratic configuration interaction (QCISD(T))-level *ab initio* points with AVTZ basis set, and the asymptotic areas were constructed by a London–Eyring–Polanyi–Sato (LEPS) function. The globally smooth PES was generated by switching from the spline-fitted *ab initio* points in the interaction region to the LEPS function near the asymptotes. The new global three-dimension adiabatic potential energy surface for the $3A''$ state calculated and fitted by Lü *et al.*

is based on more than 6000 *ab initio* points computed using the MRCI approach and a large basis set AV5Z. Hence, it is clear that the latter is more accurate.

We run 10^5 trajectories with an initial D′–DS separation distance of 10 Å in the collision energy range of 0.1–2.0 eV, and the DS reactant molecule is set in its ground rovibrational states ($v = 0$ and $j = 0$). The time integration step size of 0.1 fs is chosen to ensure the conservation of the total energy and total angular momentum. The impact parameter $b_{\max}$ is computed by calculating the whole 10^5 trajectories at a fixed value of the impact parameter b and systematically increasing the value of b until the reactive trajectories do not augment any more. The reaction cross section is defined as $\sigma_r = \pi b_{\max}^2 (N_r/N)$ (N_r, the number of reactive trajectories; N, the total number of trajectories).

3. Results and discussion

3.1. Integral cross sections

Comparison between the QM results of integral cross section by Lü *et al.* and our QCT results for the $D' + DS(v = 0, j = 0) \rightarrow D'D + S$ in the collision energy range of 0.1–2.0 eV is shown in Fig. 2. Both the current QCT calculation and previous QM study have employed the same LZHH PES. It can be obviously seen from this figure that the QCT results are in good agreement with the previous QM results in the whole range. As the collision is enhanced, the reaction cross sections rapidly reach the maximum value at $E_c = 1.2$ eV, and then decrease slightly with the further increase of collision energy. Moreover, the integral cross section exhibits an energy threshold at $E_c = 0.1$ eV due to the small barrier (0.09 eV) of the lowest triplet $^3A''$ PES. Figure 2 also indicates that there appear to be no obvious quantum effects in the integral cross section. In some reactions, such as H+HN[42] and D+H_2,[43] zero-point energy (ZPE) leakage, and tunneling have important effects. However, they have negligible influence on the title reaction.

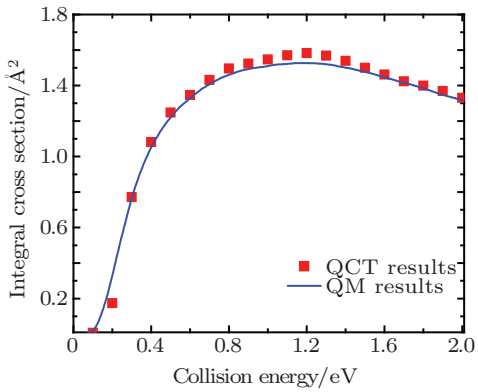


Fig. 2. (color online) Comparison between the QCT results of the integral cross section in this work and the previous QM results of the integral cross section for the $D' + DS(v = 0, j = 0) \rightarrow D'D + S$ reaction.

3.2. $P(\theta_r)$ distribution

The $P(\theta_r)$ distributions at collision energies of 0.4, 0.8, 1.2, 1.6, and 2.0 eV are presented in Fig. 3. The distribution reflects the $\boldsymbol{k}$–$\boldsymbol{j}'$ correlation of the products. In all situations, the $P(\theta_r)$ peaks at $\theta_r = 90°$ are symmetric, which manifests that the rotational angular momentum vector $\boldsymbol{j}'$ is strongly aligned along the direction perpendicular to the vector $\boldsymbol{k}$. The acquired strong rotational polarization of the product D′D molecule can be ascribed to a low barrier on the ground state $^3A''$ PES for the title abstraction reaction. Similar phenomenon can be observed in other analogical hydrogen atom abstraction reactions.[44] In addition, it is obvious in Fig. 3 that the product alignment is the weakest at 0.4 eV, and increases a little as the collision energy increases to 0.8 eV, and then remains almost invariable as the collision energy further increases. The product rotational alignment parameter $\langle P_2(\cos\theta_r)\rangle$ which can also reflect the degree of the product rotational polarization is listed in Table 1. As can be seen, the trend is well consistent with that of the $P(\theta_r)$ distributions (the more negative the expected value of $\langle P_2(\cos\theta_r)\rangle$, the stronger the rotational alignment). This relationship between the product rotational alignments and collision energies is in accord with the previous prediction by Han *et al.*[25]

Table 1. Distributions of impact parameter $b_{\max}$, number of reactive trajectories (N_r), and average value of the second Legendre moment $\langle P_2(\cos\theta_r)\rangle$ at various collision energies.

Collision energy/eV	$b_{\max}$/Å	N_r	$\langle P_2(\cos\theta_r)\rangle$
0.4	2.62	5016	–0.37805
0.8	2.665	6704	–0.38729
1.2	2.67	7070	–0.40197
1.6	2.6518	6617	–0.41042
2.0	2.67	5941	–0.42567

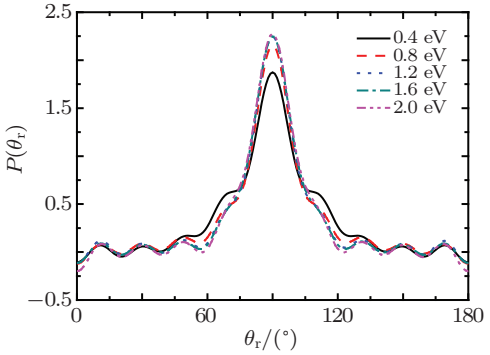


Fig. 3. (color online) Distribution of $P(\theta_r)$ describing the $\boldsymbol{k}$–$\boldsymbol{j}'$ correlation at different collision energies.

3.3. $P(\phi_r)$ distribution

The dihedral angle distributions of $P(\phi_r)$, describing the $\boldsymbol{k}$–$\boldsymbol{k}'$–$\boldsymbol{j}'$ correlation, are exhibited in Fig. 4. Because ϕ_r is the dihedral angle between the planes containing $\boldsymbol{k}$–$\boldsymbol{k}'$ and $\boldsymbol{k}$–$\boldsymbol{j}'$, the $P(\phi_r)$ can provide stereo-dynamical information on the

alignment and orientation properties of the product. It is obvious that the $P(\phi_r)$ distributions are asymmetric with respect to the $\boldsymbol{k}$–$\boldsymbol{k}'$ scattering plane (i.e., $\phi_r = 180°$). The only peak in the $P(\phi_r)$ distribution at about $\phi_r = 270°$ signifies that the product is not only aligned, but also strongly oriented along the $-y$ axis that is perpendicular to the scattering plane. In other words, the product molecules prefer a left-handed rotation in planes parallel to the scattering plane. The strong peaks around $\phi_r = 270°$ indicate the repulsive character of the PES.[44] As shown in Fig. 4, the orientation of product molecules show a reduction trend at high energies, since the $\phi_r = 270°$ peak becomes weaker and broader with increasing collision energy. This denotes that the product molecule rotation changes from the in-plane mechanism to out-of-plane mechanism. According to the previous studies of a reactive system of light–light–heavy (LLH) mass combination,[45] the product orbital angular momentum $\boldsymbol{L}'$ is mostly derived from the reactant orbital momentum $\boldsymbol{L}$, and $\boldsymbol{j}'$ is almost independent of $\boldsymbol{L}$. A great deal of collision energy transfers into the translational energy of the product, and the contribution to the product rotation angular momentum is small. Moreover, the D′D product can rapidly and effortlessly move away from the heavy S atom in the same direction as the reagent D′ atom when the collision energy is high enough, which will be discussed in detail below. Therefore, the orientation of product molecular rotational angular momentum exhibits a contraction with increasing collision energy.

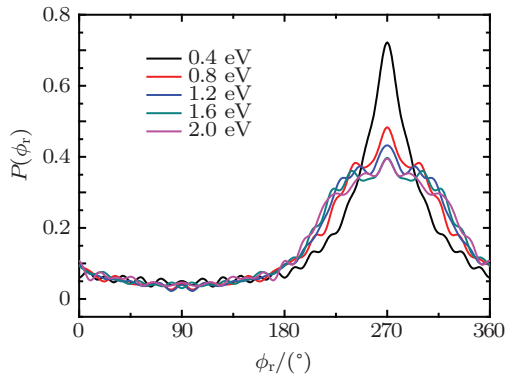


Fig. 4. (color online) Distribution of $P(\phi_r)$ reflecting the $\boldsymbol{k}$–$\boldsymbol{k}'$–$\boldsymbol{j}'$ correlation at different collision energies.

3.4. Joint $P(\theta_r, \phi_r)$ distribution

In order to further verify the above tendencies connected with the collision energy effect on the $P(\theta_r)$ and $P(\phi_r)$ distributions, the joint distributions $P(\theta_r, \phi_r)$ at $E_c = 0.4$, 0.8, 2.0 eV are plotted in Fig. 5, which have a sensitive dependence on the collision energy. It is also clear that $P(\theta_r, \phi_r)$ has a peak at (90°, 270°), which is in good accordance with the distributions of $P(\theta_r)$ and $P(\phi_r)$. The product molecules tend to be perpendicular to the scattering plane and rotate out of planes with increasing collision energies.

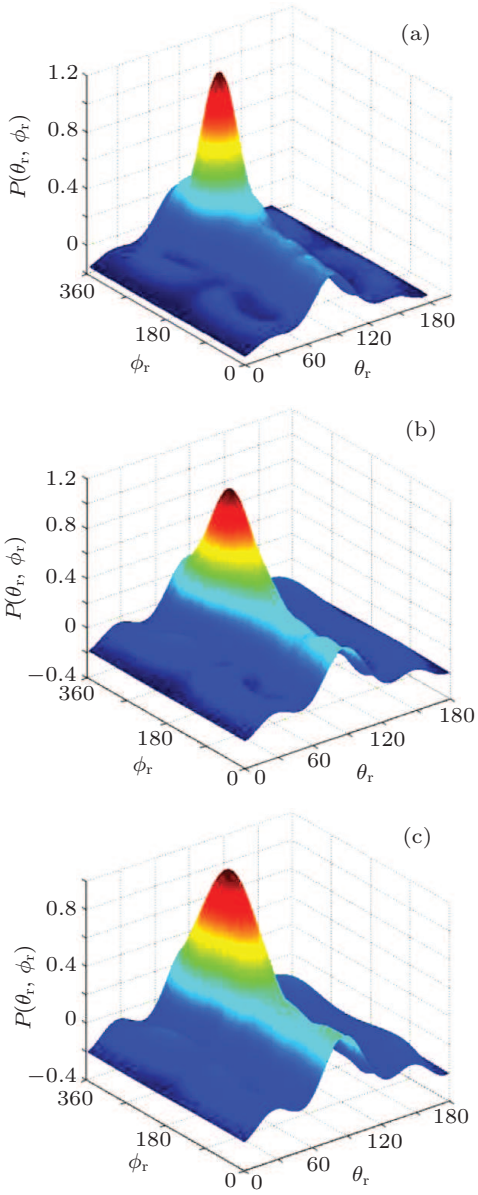


Fig. 5. (color online) The joint probability density distribution $P(\theta_r, \phi_r)$ as a function of both θ_r and ϕ_r at three collision energies. (a) E_c = 0.4 eV, (b) $E_c = 0.8$ eV, and (c) $E_c = 2.0$ eV.

3.5. PDDCSs

The calculated PDDCSs ($(2\pi/\sigma)(d\sigma_{00}/d\omega_t)$, $(2\pi/\sigma)(d\sigma_{20}/d\omega_t)$, $(2\pi/\sigma)(d\sigma_{22+}/d\omega_t)$, $(2\pi/\sigma)(d\sigma_{21-}/d\omega_t)$) as functions of both collision energy and scattering angle θ_t are plotted in Fig. 6. As well known, the $PDDCS_{00}$ is simply the ($\boldsymbol{k}$, $\boldsymbol{k}'$) differential cross section (DCS). It can be seen from Fig. 6(a) that the D′D molecule shows broad backward-sideway dispersion at low collision energy of 0.4 eV. Then, the angular distributions evolve toward the forward direction as the collision energy increases. At high collision energy of 2.0 eV, the present DCS is dominant in forward scattering directions with a peak at $\theta_t = 54°$. Similar results have also been observed in F+HCl[46] and H′+HBr reactions.[44]

To further explore the reasons for different DCS features at different collision energies, the internuclear distances of D′S, DS, and D′D as functions of propagation time at $E_c = 0.4$,

1.2, and 2.0 eV are presented in Fig. 7. The trajectories plotted here are chosen randomly. As shown in Fig. 7, the D′ atom moves straight toward the DS molecule, generating a D′D product that recoils immediately. Apparently, the required time for the generation of product D′D is about 0.14 ps at $E_c = 0.4$ eV, and then decreases to less than 0.1 ps at $E_c = 2.0$ eV. This indicates that the trajectories keep close to the minimum energy reaction path and obey a direct reaction mechanism, which is ascribed to the single low barrier along the reaction process. At low collision energies, the D′D product with small momentum can be bounced back easily by the heavy S atom. As the collision energy grows, the D′D product gains more internal energy and can move with little or no interference from the heavy S atom along the original direction of the reagent D′ atom. This explains the backward/sideways angular distributions at $E_c = 0.4$, 0.8, 1.2 eV and the forward distributions at $E_c = 1.6$, 2.0 eV.

The PDDCS_{20} related to the expected value $\langle P_2(\cos\theta_r)\rangle$ are drawn in Fig. 6(b). The opposite trend to that of PDDCS_{00} in Fig. 6(a) implies that the product rotational alignment is perpendicular to $\boldsymbol{k}$. This is in accordance with the product alignment of the $P(\theta_r)$ distribution, depicted in Fig. 3.

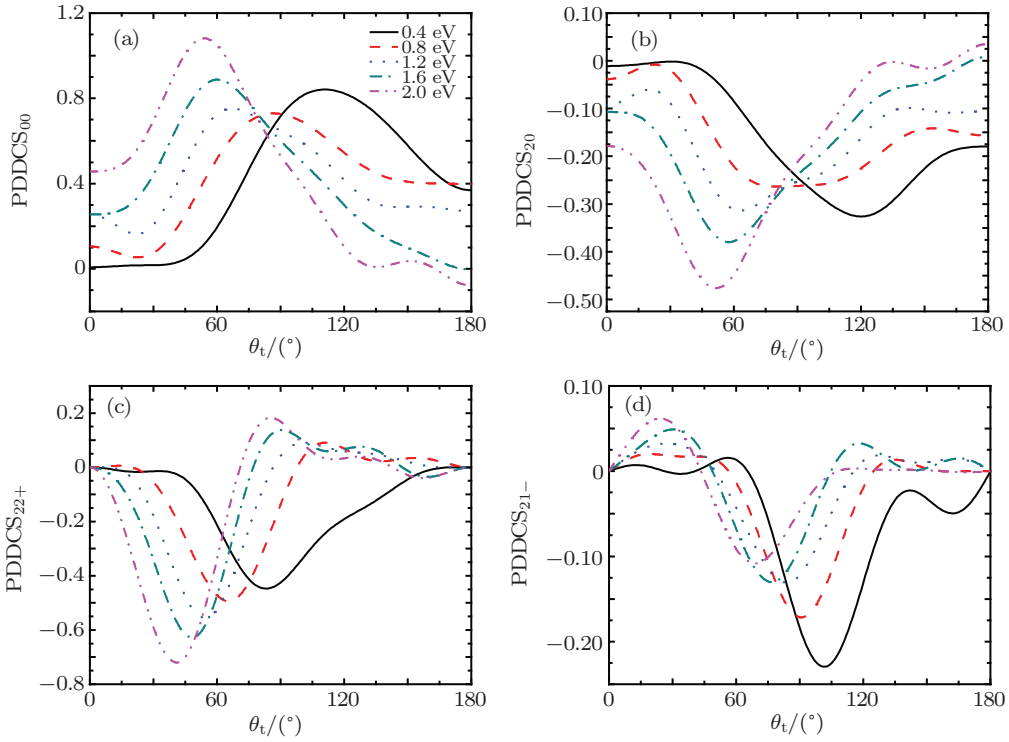


Fig. 6. (color online) Differential cross sections of PDDCSs as functions of the scattering angle. (a) PDDCS_{00}, (b) PDDCS_{20}, (c) PDDCS_{22+}, and (d) PDDCS_{21-}.

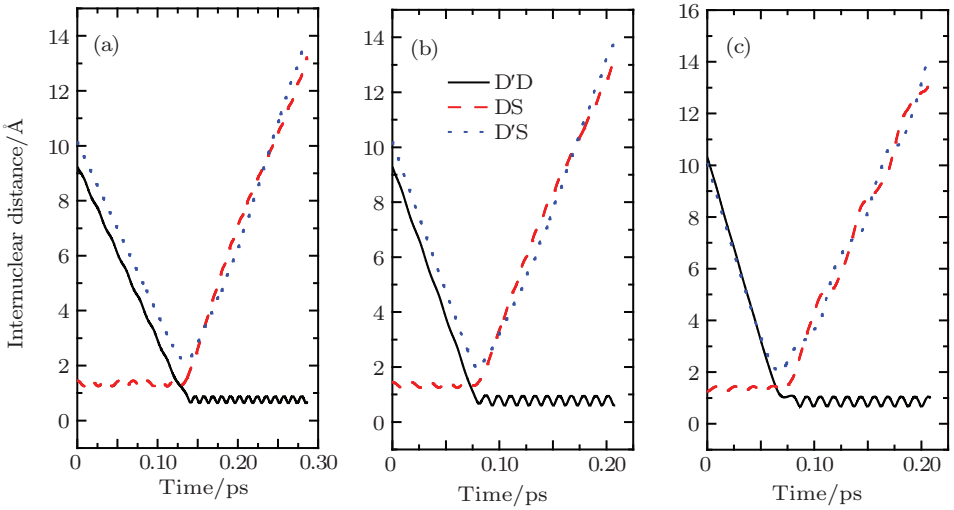


Fig. 7. (color online) Internuclear distances of D′D, DS, and D′S as functions of propagation time at (a) $E_c = 0.4$ eV, (b) $E_c = 1.2$ eV and (c) $E_c = 2.0$ eV.

The angular distribution PDDCSs with $q \neq 0$ are drawn in Figs. 6(c) and 6(d). All PDDCSs with $q \neq 0$ are equal to zero at the extremities of forward and backward scattering. The negative value of $PDDCS_{22+}$, which is related to $\langle \sin^2\theta_r \cos 2\phi_r \rangle$, implies the product alignment is along the y axis, while the positive value implies the product alignment is along the x axis. In Fig. 6(c), it can be seen that the $PDDCS_{22+}$ is negative for all scattering angles when the collision energy is 0.4 eV, which indicates the remarkable preference of product alignment along the y axis. With the increase in the collision energy, the $PDDCS_{22+}$ distributions show more transparent anisotropy. It is obvious that at the collision energy of 0.8 eV, the $PDDCS_{22+}$ values are negative at the scattering angles below about 100° and positive at other scattering angles. A similar situation can be found for the collision energy of 1.2 eV that the $PDDCS_{22+}$ values are slightly positive at the scattering angles above about 86° and negative at other scattering angles. This indicates that the alignments of the D′D product are along both the x axis and the y axis, but dominantly along the y axis. For $E_c = 1.6$ and 2.0 eV, a similar behavior can be observed. The values of $PDDCS_{22+}$ are positive for the scattering angle ranges of 76° –147° and 70°–143°, and negative at other scattering angles, which indicates the remarkable preference of product alignment along the x axis and the y axis at these scattering angles, respectively. The value of $PDDCS_{21-}$ correlates to $\langle -\sin 2\theta_r \cos\phi_r \rangle$, and its behavior is analogous to that of the $PDDCS_{22+}$. The $PDDCS_{21-}$ is positive or negative, corresponding to the product rotational angular momentum $\boldsymbol{j}'$ along the directions of vector $\boldsymbol{x}$–$\boldsymbol{z}$ or $\boldsymbol{x}+\boldsymbol{z}$. As shown in Fig. 6(d), the $PDDCS_{21-}$ values oscillate moderately at different scattering angles with increasing collision energies. It is demonstrated that the anisotropic feature of the D′D products is less obvious at high collision energies. We can note that the values of the $PDDCS_{21-}$ distributions are negative in most region, and the positive values of the $PDDCS_{21-}$ are about zero, which indicates that j' prefers to align along the $\boldsymbol{x}+\boldsymbol{z}$ directions. Meanwhile, the shrinking trend of the negative peak shows that the product polarization becomes weaker as the collision energy increases.

4. Conclusions

In summary, the QCT calculations have been carried out to investigate the collision energy influence on the dynamics of the abstraction reaction $D' + DS(v = 0, j = 0) \rightarrow D'D + S$ on ground $^3A''$ PES. It has been found that the present integral cross sections are well consistent with the available results of QM calculations. The calculated results indicate the repulsive character of the new fitted LZHH PES. The direct reaction mechanism plays a dominant role in the total reaction process in the considered range of the collision energy. The results of the $P(\theta_r)$ and $P(\phi_r)$ distributions reveal that the product rotational angular momentum vectors $\boldsymbol{j}$ are not only aligned, but also oriented. The product rotational alignments are changed a little, while the orientation effects become weaker with increasing collision energy. The calculated four PDDCSs show the preference of scattering forward of the product, and the weaker tendency of the polarization with the increase in the collision energy.

Acknowledgements

The authors are very grateful to Prof. Han Ke-Li for providing the QCT code. The authors also acknowledge Dr. Lü Shuang-Jiang , Li Wen-Liang, and Duan Zhi-Xin for their useful advice.

References

[1] Chu T S, Han K L and Schatz G C 2007 *J. Phys. Chem. A* **111** 8286
[2] Banares L, Castillo J F, Honvault P and Launay J M 2005 *Phys. Chem. Chem. Phys.* **7** 627
[3] Klos J A, Dagdigian P J and Alexander M H 2007 *J. Chem. Phys.* **127** 154321
[4] Maiti B, Schatz G C and Lendvay G 2004 *J. Phys. Chem. A* **108** 8772
[5] Yang H, Han K, Schatz G C, Smith S C and Hankel M 2010 *Phys. Chem. Chem. Phys.* **12** 12711
[6] Chu T S and Han K L 2008 *Phys. Chem. Chem. Phys.* **10** 2431
[7] Chu T S, Zhang X and Han K L 2005 *J. Chem. Phys.* **122** 214301
[8] Chu T S, Zhang Y and Han K L 2006 *Int. Rev. Phys. Chem.* **25** 201
[9] Shiina H, Miyoshi A and Matsui H 1998 *J. Phys. Chem. A* **102** 3556
[10] Tsuchiya K, Yamashita K, Miyoshi A and Matsui H 1996 *J. Phys. Chem.* **100** 17202
[11] Martin R L 1983 *Chem. Phys.* **82** 337
[12] Ho T S, Hollebeek T, Rabitz H, Der Chao S, Skodje R T, Zyubin A S and Mebel A M 2002 *J. Chem. Phys.* **116** 4124
[13] Lü S J, Zhang P Y, Han K L and He G Z 2012 *J. Chem. Phys.* **136** 094308
[14] Lü S J, Zhang P Y and He G Z 2012 *Chin. Phys. Lett.* **29** 073401
[15] Wang T and Yue X F 2011 *Chin. Phys. Lett.* **28** 023101
[16] Zhao J and Luo Y 2011 *Chin. Phys. B* **20** 043402
[17] Liu Y F, Liu Y L and Liang B 2012 *Chin. Phys. B* **21** 098201
[18] Xu Z H, Zong F J, Han B R, Dong S H, Liu J Q and Ji F 2012 *Chin. Phys. B* **21** 093103
[19] Yue X F 2012 *Chin. Phys. B* **21** 073401
[20] Ge M H and Zheng Y J 2011 *Chin. Phys. B* **20** 083401
[21] Liu S L and Shi Y 2011 *Chin. Phys. B* **20** 013404
[22] Orr-Ewing A J and Zare R N 1994 *Ann. Rev. Phys. Chem.* **45** 315
[23] Han K L, Zheng X G, Sun B F, He G Z and Zhang R Q 1991 *Chem. Phys. Lett.* **181** 474
[24] Aquilanti V, Bartolomei M, Pirani F, Cappelletti D, Vecchiocattivi F, Shimizu Y and Kasai T 2005 *Phys. Chem. Chem. Phys.* **7** 291
[25] Han K L, He G Z and Lou N Q 1996 *J. Chem. Phys.* **105** 8699
[26] Chen M D, Tang B Y, Han K L and Lou N Q 2001 *Chem. Phys. Lett.* **337** 349
[27] Wang M L, Han K L and He G Z 1998 *J. Chem. Phys.* **109** 5446
[28] Li W L, Wang M S, Yang C L, Ma X G, Wang D H and Liu W W 2007 *Chem. Phys. Lett.* **445** 125
[29] Kang L H and Zhu M Y 2010 *J. Mol. Struct.-THEOCHEM* **945** 116
[30] Han B R, Zong F J, Wang C L, Ma W Y and Zhou J H 2010 *Chem. Phys.* **374** 94
[31] Meng Q T, Zhao J, Xu Y and Yue D G 2009 *Chem. Phys.* **362** 65
[32] Wei Q, Li X and Li T 2010 *Chem. Phys.* **368** 58
[33] Xu W W, Liu X G, Luan S X and Zhang Q G 2009 *Chem. Phys.* **355** 21
[34] Zhang J, Chu T S, Dong S L, Yuan S P, Fu A P and Duan Y B 2011 *Chin. Phys. Lett.* **28** 093403
[35] Zhao J, Xu Y and Meng Q T 2009 *J. Phys. B* **42** 165006
[36] Li X H, Wang M S, Pino I, Yang C L and Ma L Z 2009 *Phys. Chem. Chem. Phys.* **11** 10438
[37] Xiao J, Yang C L, Tong X F, Wang M S and Ma X G 2011 *J. Phys. Chem. A* **115** 1486
[38] Yue X F, Zhang Y Q, Feng H R and Wu E L 2010 *J. Mol. Struct.-THEOCHEM* **955** 61
[39] Chu T S, Zhang H, Yuan S P, Fu A P, Si H Z, Tian F H and Duan Y B 2009 *J. Phys. Chem. A* **113** 3470
[40] Yu Y J, Xu Q and Xu X W 2011 *Chin. Phys. B* **20** 123402
[41] Aoiz F J, Brouard M and Enriquez P A 1996 *J. Chem. Phys.* **105** 4964
[42] Han B R, Yang H, Zheng Y J and Varandas A J C 2010 *Chem. Phys. Lett.* **493** 225
[43] Ju L P, Han K L and Zhang J Z H 2009 *J. Comput. Chem.* **30** 305
[44] Zhang W Q, Cong S L, Zhang C H, Xu X S and Chen M D 2009 *J. Phys. Chem. A* **113** 4192
[45] Wang M L, Han K L and He G Z 1998 *J. Phys. Chem. A* **102** 10204
[46] Duan Z X, Li W L and Qiu M H 2012 *J. Chem. Phys.* **136** 144309